Tribology International, V. 167, 2022, 107398, DOI: 10.1016/j.triboint.2021.107398 (Accepted version)

Transient non-Newtonian Elastohydrodynamics of Rough Meshing Hypoid Gear Teeth Subjected to Complex Contact Kinematics

Gajarajan Sivayogan[1], Ramin Rahmani[1*] and Homer Rahnejat[2]

[1] Wolfson School of Mechanical, Electrical and Manufacturing Engineering, Loughborough University, Leicestershire LE11 3TU, UK

[2] School of Engineering, University of Central Lancashire, Preston PR 1 2HE, UK

*Corresponding author: R.Rahmani@lboro.ac.uk

Abstract

Predictions are provided for mixed elastohydrodynamic conditions of meshing hyoid gear teeth pairs of light truck differentials. Under transient conditions, pertaining to vehicle cruising or in urban driving, the lubricant is subjected to non-Newtonian traction. The meshing teeth are subjected to complex kinematics, comprising rolling, sliding and squeeze film motions. Furthermore, instantaneously varying angled lubricant flow into the contact constitutes a precession of contact footprint, further complicating the prevailing conditions. The inclusion of all these interacting kinematics shows that the lubricant film thickness, shear characteristics and transmission efficiency are significantly affected by the ensuing transience. This cannot be adequately represented by the usual quasi-steady analyses. The in-depth detailed analysis of the hypoid gear pairs of vehicular differentials constitutes the main contribution of the paper.

Keywords: Vehicular differential; Hypoid Gears; Transient mixed elastohydrodynamics; Non-Newtonian shear

1. Introduction

Bevel or hypoid gears are key components of vehicular differentials, transmitting the engine power through $90°$ transformation to the driven axle. With a strong global consensus and stringent regulations and directives to reduce emissions, it is important for automotive manufacturers to improve upon drivetrain energy efficiency. This can be achieved through reduced frictional losses, whilst guarding against any emerging untoward Noise, Vibration and Harshness (NVH) phenomena [1,2]. Therefore, it is essential to enhance the understanding of tribodynamics of hypoid and bevel gears under transient driving conditions.

The contact of bevel and hypoid gear teeth pairs is subjected to elliptical point contact elastohydrodynamic regime of lubrication (EHL) [3]. An early investigation of power losses of hypoid gear pairs was carried out by Xu and Kahraman [4]. They assumed Newtonian shear of the lubricant for the determination of viscous shear and thus contact friction. Simon [5] found that EHL is overly sensitive to misalignment, particularly for face-hobbed spiral bevel gears. In a more recent study, the same author focused on mixed-EHL regime of lubrication [6]. With a focus on manufacturing parameters, he showed that head-cutter modifications could be optimised such that the maximum EHL pressure would be reduced. However, he noted that such modifications only marginally improved the overall efficiency of hypoid gears. Furthermore, for hypoid gear teeth pairs' contacts the inlet lubricant entrainment often

occurs at an angle to the elliptical contact footprint axes as shown by Mohammadpour et al [7]. This implies that under transient conditions the contact footprint would be subjected to precession (spin) if the direction of inward flow would be regarded as fixed. Later, the same authors showed that lubricant film thickness, based on the use of extrapolated oil film expressions, is somewhat overestimated [8], as these expressions are usually from regression of results based on assumed fully flooded inlets, isothermal conditions, and Newtonian traction [9]. In reality, particularly at high shear, the contact conditions are non-Newtonian thermal, invariably with a starved inlet due to reverse and recirculating flows at the inlet meniscus [10]. Therefore, realistic representation of contact kinematics under transient conditions is critical in any predictive analysis.

There have been a number of studies of contact footprints subjected to spin. An early study was carried out by Mostofi and Gohar [11] for pure spin under isothermal EHL. They showed that the influence of spin becomes significant at higher angular velocities. Later, Ehret et al [12] studied the traction behaviour in EHL contacts under the influence of spin with shear thinning of the lubricant. They showed that for low slide-roll ratios (less than 0.02), the influence of spin becomes significant. Ehret et al [12] showed that there can be a reduction in traction when spin motion is included in the analysis, compared with a no spin. Li et al [13] showed that at higher loads the lubricant film thickness, and particularly the location and magnitude of the contact side lobes are influenced by any spinning motion of the contact footprint. Dormois et al [14] also studied the effect of spin in a more advanced manner; considering the speed of lubricant entrainment into the contact in 3 stages: an initial linear entrainment velocity, as well as transverse and longitudinal components induced by the introduction of spin. They showed that the classical idealised symmetry of film thickness is lost due to any changes in pressure-induced spinning motion. Doki-Thonon et al [15] provided experimental and numerical examples using a relatively new apparatus, 'Tribogyr'. The authors observed that the non-uniform velocity fields, induced by spin action, can produce a local maximum on the film thickness contours close to the exit constriction of the contact. In a recent study using a thermoelastohydrodynamic (TEHL) model with the consideration of mixed and boundary lubrication, Yan et al [16] also explored the effect of spin, aiming to replicate similar operating conditions as those in Continually Variable Transmissions (CVT). The authors' focus was on the effect of fatigue life induced by any spinning of the contact footprint.

The contact of meshing teeth is subjected to complex kinematics, including rolling, and sliding, and as already described some degree of precession. Under transient conditions, there is also the mutual approach and separation of teeth pairs which promotes squeeze film motion [17, 18]. Squeeze action is also promoted by any rise and fall in the film thickness as the result of changes in loading, surface geometry, speed of entraining motion, as well as any reciprocating motion in many applications [19, 20]. Squeeze film action, in the mutual convergence of mating surfaces, as well as under impacting conditions promotes increased load carrying capacity of the contact as observed by the formation of a squeeze cave, sometimes referred to as a dimple [21-25]. In the case of gear teeth, the geometry of contacting flanks alters instantaneously during a meshing cycle, together with the surface sliding and rolling velocities as well as the applied contact load. Therefore, the effect of squeeze film motion is important and should be considered by including it in Reynolds' equation. Larsson [26] showed that for the case of spur gears, squeeze film motion is only marginally influenced by the instantaneous radii of curvature of the meshing flanks and their surface speeds, and that the transience is mostly affected by the load applied on the contacting teeth. However, numerous studies of EHL contacts have also shown the dominance of squeeze film motion which occurs as the result of changes in surface speeds of contacting solids, more so than any

applied load variation which the EHL films are actually rather insensitive to [27-29]. It should also be noted that Larsson [26] assumed isothermal conditions, although his model incorporated non-Newtonian effects. A more detailed analysis for thermoelatohydrodynamic analysis of spur gears was reported by Sivayogan et al [30] who used a thermal network model, integrated with tooth contact analysis to precisely include the effect of instantaneous radii of curvature of surfaces. However, the analysis did not include the effect of squeeze film motion.

Other studies of spur gears, including the effect of asperity interactions as well as squeeze film motion have included those of Li and Kahraman [31, 32], who focused on determining the potential power losses. Later, using theoretical tooth profiles, Li and Kahraman [33] showed the essential coupling between gear dynamics and tribology of contact throughout the meshing cycle. The authors included the effects of non-linear dynamics and found that tooth separation caused by backlash has a profound effect upon the elastohydrodynamic contact. The linkage between gear dynamics and contact kinematics was also taken into account by Mohammadpour et al [34] and Paouris et al [35]. However, their analyses ignored the effects of squeeze film motion and contact spin. Koronias et al [2] also showed that contact separation leads to reduced friction/traction with the remaining excess energy in the vehicular differentials inducing an NVH phenomenon termed as axle whine.

Bobach et al [36] studied spiral bevel gear meshing teeth which have similar geometry, but different loading characteristics to the hypoid gears [37]. They focused on the transient behaviour with lubricant shear thinning effect, also including asperity interactions of the real rough gear teeth counter faces. They also used a comprehensive thermal model. Whilst the authors included the effect of angled inlet flow lubricant entrainment into the contact, they did not consider the effect of contact footprint precession in a transient manner. Nevertheless, they showed that in certain parts of the meshing cycle a spiral bevel gear pair runs predominantly in mixed-EHL regime of lubrication, even when some degree of squeeze was considered. Their findings emphasise the need for a similar in-depth analysis for the case of hypoid gears. Additionally, an important issue is an accurate determination of instantaneous radii of curvature of the meshing teeth using Tooth Contact Analysis.

Hitherto, none of the reported analyses has dealt with the transient non-Newtonian EHL of hypoid gear teeth pairs under realistic complex combined contact kinematics, comprising rolling/sliding, mutual approach and separation (i.e., squeeze film effect) and precession of the contact during meshing of a pair of hypoid gear teeth. This paper provides such an in-depth analysis by extending the reported methodologies in [29, 30], also incorporating Tooth Contact Analysis (TCA) and boundary interaction of rough flank surfaces (i.e., transient mixed non-Newtonian EHL).

2. Methodology

2.1 Governing Equations

The general transient two-dimensional form of Reynolds equation with lubricant flow at an angle to an elliptical contact footprint is given as:

$$\frac{\partial}{\partial x}\left[\frac{\rho h^3}{6\eta}\left(\frac{\partial p}{\partial x}\right)\right]+\frac{\partial}{\partial y}\left[\frac{\rho h^3}{6\eta}\left(\frac{\partial p}{\partial y}\right)\right]=\frac{\partial(\rho h U)}{\partial x}+\frac{\partial(\rho h V)}{\partial y}+\frac{\partial(2\rho h)}{\partial t} \quad (1)$$

where, h, p, η and ρ are the film thickness, generated pressure, lubricant dynamic viscosity and density, respectively. The coordinate system is so chosen such that the x-axis remains along the minor axis of the

elliptical contact footprint, whilst the y-axis is in the direction of its major semi-half-width. Surface speeds for the case with no contact spin condition; U and V become:

$$U = u_p + u_g \tag{2}$$

$$V = v_p + v_g \tag{3}$$

where, u_p, u_g, v_p and v_g are found by undertaking Tooth Contact Analysis; a brief description of which is provided in section 2.2.

The ultimate term in Reynolds' equation, $\partial(2\rho h)/\partial t$, corresponds to the lubricant squeeze film motion. As already noted, most studies concerning the analysis of hypoid gears' meshing teeth pairs have neglected this term. Thus, the transient nature of the lubricated contact is not properly accounted for. Furthermore, in such cases, the effect of squeeze film motion on the contact load carrying capacity has not hitherto been included.

The instantaneous elastic film shape is given as:

$$h(x, y) = h_0 + s(x, y) + \delta(x, y) \tag{4}$$

where, h_0 is the minimum clearance between the two undeformed geometrical profile and s is the geometrical profile of contact between an equivalent ellipsoidal solid against a semi-infinite elastic half-space (figure 1) [3, 38], represents the instantaneous contact made between the two meshing gear teeth with variable geometries (radii of curvature):

$$s = \frac{x^2}{2R_{zx}} + \frac{y^2}{2R_{zy}} \tag{5}$$

where, the radii of curvature of the equivalent ellipsoidal solid in figure 1 along the principal planes of contact are:

$$\frac{1}{R_{zx}} = \frac{1}{R_{x1}} + \frac{1}{R_{x2}}, \qquad \frac{1}{R_{zy}} = \frac{1}{R_{y1}} + \frac{1}{R_{y2}} \tag{6}$$

The instantaneous radii of the meshing surfaces in the principal planes of contact; R_{x1}, R_{x2}, R_{y1} and R_{y2} are determined through TCA for any instant of meshing within a meshing cycle of a teeth pair.

The equivalent (reduced) Young's modulus of elasticity of the semi-infinite elastic half-space is given as:

$$\frac{2}{E'} = \frac{1-\nu_1^2}{E_1} + \frac{1-\nu_2^2}{E_2} \tag{7}$$

where, $E_{1,2}$ and $\nu_{1,2}$ are the Young's moduli of elasticity and Poisson's ratios of the contacting pairs.

The localised contact elastic deflection, δ, in equation (4) is given by the elasticity potential equation as [28]:

$$\delta = \frac{2}{\pi E'} \iint \frac{p(x', y')}{\sqrt{(x-x')^2 + (y-y')}} dx' dy' \tag{8}$$

where, (x', y') is the coordinate of the point of application of a generated elemental contact pressure and (x, y) is the resulting localised deflected position.

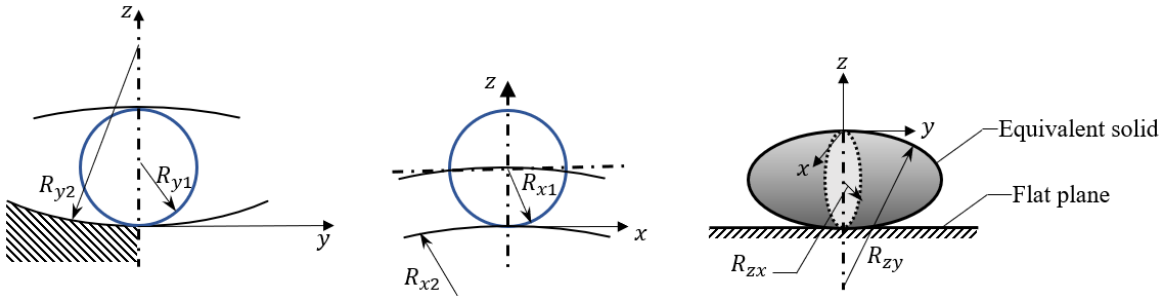

Figure 1: The equivalent instantaneous ellipsoidal solid of revolution contacting a semi-infinite elastic half-space

It has been shown by many authors that most gear pairs, and particularly hypoid gear pairs at high load and shear, operate under non-Newtonian elastohydrodynamic conditions [4, 6, 8, 26, 30, 35]. Therefore, it is necessary to use a non-Newtonian viscosity model, such as that highlighted in [30, 35, 39], who have all used the Havriliak and Negami [40] rheological model to include the effect of shear thinning:

$$\eta = \frac{\eta_0}{F(\lambda_f)} \tag{9}$$

where, η_0 is the atmospheric dynamic viscosity. The non-Newtonian function, $F(\lambda_f)$, and shear rate, $\dot{\gamma}$, are given as:

$$F(\lambda_f) = \left[1 + (\lambda_f \dot{\gamma})^{\alpha_{HN}}\right]^{\beta_{HN}} \tag{10}$$

where the shear rate is approximated at:

$$\dot{\gamma} = \frac{\Delta U}{h_c} \tag{11}$$

In addition, λ_f, α_{HN}, β_{HN} are the lubricant-specific parameters, found experimentally [41]. The shear rate is calculated using the lubricant film thickness at the centre of the meshing teeth pair contact footprint, h_c. It has been shown that for most of the meshing cycle of hypoid gear teeth pairs the lubricant undergoes viscoelastic traction [8, 35]. Therefore, the lubricant viscosity would still be highly dependent on the generated contact pressures, and thus the Havriliak and Negami model [40] needs to be adjusted accordingly:

$$\eta = \frac{\eta_p}{F(\lambda_f)} \tag{12}$$

where, η_p can be found using the standard Roelands' equation [42]:

$$\eta_p = \eta_e \exp\left\{\ln\left(\frac{\eta_0}{\eta_r}\right)\left[\left(1 + \frac{p}{p_r}\right)^Z - 1\right]\right\} \tag{13}$$

where, η_r and p_r are 6.31×10^{-5} and 1.9609×10^8 respectively, and η_e is the effective dynamic viscosity of the lubricant at the operating temperature, determined through use of Vogel's equation [43]:

$$\eta_{\mathrm{e}} = a_v \exp\left(\frac{b_v}{T - c_v}\right) \tag{14}$$

where, the lubricant-specific constants a_v, b_v and c_v are found by measuring viscosity at three different temperatures and performing the subsequent curve-fitting. Table 1 shows the constants used for this analysis.

The piezo-viscosity index, *Z*, in equation (13) is obtained as:

$$Z = \frac{\alpha_0 p_r}{\ln\left(\frac{\eta_0}{\eta_r}\right)} \tag{15}$$

where, α_0 is the experimentally determined pressure–viscosity coefficient.

Table 1: Vogel constants for the lubricant in the current analysis [35]

Symbol	Value	Unit
a_v	1.55×10^{-4}	Pa.s
b_v	944	K
c_v	165.2	K

Lubricant density also alters with temperature and pressure [44]:

$$\rho = \rho_0 \left(1 + \frac{0.6\times10^{-9} p}{1+1.7\times10^{-9} p}\right)[1 - 0.65 \times 10^{-3}(T - T_0)] \tag{16}$$

where, ρ_0 is the density of lubricant at atmospheric pressure and room temperature.

2.2 Tooth Contact Analysis (TCA)

TCA is used to obtain the contact footprint geometry, the principal radii of contact of the meshing flanks and the corresponding contact kinematics throughout a meshing cycle. A brief description of TCA is highlighted here for the sake of completeness. More detailed descriptions are provided elsewhere [30, 45- 47]. Essentially, TCA determines the direction and magnitude of surface velocities for each meshing flank. This is achieved through discretisation of flank profiles, whilst solving the equations of motion for all the discretised positions. The teeth flank surfaces are usually predetermined from theoretical manufacturing data [45].

TCA outputs the position vector $\overline{r_{s_i}}$ for all the contact points at any instant of time, where the subscript s_i refers to either p or g, denoting pinion or gear wheel, respectively. For all the corresponding points, unit vectors of both the major $\hat{a}$ and minor $\hat{b}$ axes of the contact ellipse are also obtained for any given angular velocity of the pinion, ω_p, and the gear wheel, ω_g . Therefore, it is possible to calculate the surface speeds with respect to the minor, u_{s_i}, and the major, v_{s_i}, axes of the contact footprint [45-47]:

$$u_{s_i} = \omega_{s_i}\left(\hat{b} \cdot \left(\hat{k}_{s_i} \times \overline{r_{s_i}}\right)\right) \tag{17}$$

$$v_{s_i} = \omega_{s_i}\left(\hat{a}\cdot\left(\hat{k}_{s_i}\times\overline{r_{s_i}}\right)\right) \tag{18}$$

where, $\hat{k}$ is the unit vector along the axis of rotation for either the pinion or the gear.

It must be noted that the position vector, $\overline{r_g}$, is determined by the TCA. However, due to the nature of hypoid gears, the pinion has an offset, which needs to be accounted for prior to the use of the above stated equations.

A simple transformation matrix, M, can be applied onto the position vector, $\overline{r_g}$, in order to determine, $\overline{r_p}$ as:

$$\overline{r_p} = M\overline{r_g} \tag{19}$$

where,

$$M = \begin{bmatrix} 1 & 0 & 0 & -\text{offset} \\ 0 & 1 & 0 & 0 \\ 0 & 0 & 1 & 0 \\ 0 & 0 & 0 & 1 \end{bmatrix} \tag{20}$$

2.3 Numerical solution procedure

The following procedure is used to solve the governing and constitutive equations:

1. Contact geometry (from TCA), lubricant rheology and operating conditions such as loading conditions were used as input parameters at any instant of meshing.
2. An initial guess was made for the minimum film thickness at the centre of the contact. No squeeze film motion is initially assumed at the outset of the iterative process.
3. The computational domain was set with geometric definitions and spin coordinates as outlined in Figure 1.
4. Generated pressures, localised elastic deformation, corresponding lubricant film shape and lubricant rheological state equations were solved using Effective Influence Newton-Raphson (EIN) under-relaxation method, with the iterative pressures updated as:

   $$p^n = p^{n-1} + \Omega\Delta p^n \tag{21}$$

   where, Ω is the under-relaxation factor and in this analysis: $\Omega = 10^{-2}$.

5. At any instant of time within the meshing cycle, the pressure iterations are achieved when the following convergence criterion is met:

   $$\sum_i\sum_j\left|\frac{p_{i,j}^n - p_{i,j}^{n-1}}{p_{i,j}^n}\right| \le e_p \tag{22}$$

   where convergence limit, e_p =10^{-5}.

6. The total contact load carrying capacity comprised of W_p, the load carried by the thin film of lubricant under EHL conditions and W_{asp}, due to direct contact of counter face asperities, is obtained as:

$$W_p = \iint p\, dxdy \tag{23}$$

$$W_{asp} = \frac{8\sqrt{2}}{15}\pi(\xi_c\beta_c\sigma_c)^2\sqrt{\frac{\sigma_c}{\beta_c}}E'A_tF_{\frac{5}{2}}(\lambda_s) \tag{24}$$

where, A_t is the total apparent area of contact. The composite Greenwood and Tripp [48] roughness parameters ξ_c, β_c and σ_c are chosen for this investigation based on the measured data in [35,49] and presented in Table 2. The statistical function $F_{5/2}$ can be represented by a polynomial function as [50]:

$$F_{\frac{5}{2}}(\lambda_s) = -0.0046\lambda_s^5 + 0.0574\lambda_s^4 - 0.2958\lambda_s^3 + 0.7844\lambda_s^2 - 1.0776\lambda_s + 0.6167 \tag{25}$$

where, the local Stribeck's lubricant film ratio is given as:

$$\lambda_s = \frac{h(i,j)}{\sigma_c} \tag{26}$$

7. At any instant of meshing the following equilibrium condition should be satisfied:

$$\left|\frac{W-W_t}{W}\right| \leq e_w \tag{27}$$

where, W is the applied load (from TCA) and W_t is the total contact reaction as the sum of W_p and W_{asp}. The load convergence limit $e_w = 10^{-3}$.

8. If the stated equilibrium condition is not met, then the lubricant film thickness is updated as:

$$h_0 = h_0\left(\frac{W_p}{W}\right)^{\zeta} \tag{28}$$

where, ς is the damping/load relaxation factor, which is 0.1 for quasi-steady conditions and 0.005 for transient analysis.

Steps 4 to 8 are repeated until instantaneous equilibrium conditions are met.

9. Load and lubricant entrainment speed are updated for any successive iteration step.
10. Squeeze velocity is calculated based on the chosen time step, using pressure, film thickness and density from the previous time step and that of the newly calculated current values.

Table 2: Roughness parameters [35,49]

Symbol	Value	Units
β_c	0.7471	μm
ξ_c	0.0313×10^{12}	m^{-2}
σ_c	0.2	μm

2.4 Computational domain and kinematics of contact

For transient analysis it is important to consider the squeeze term, $\partial(\rho h)/\partial t$, in the Reynolds equation. This embodies the variation of film thickness with time, such as during a meshing cycle:

$$\frac{\partial(\rho h)}{\partial t} = \frac{\partial \rho}{\partial t} h + \frac{\partial h}{\partial t} \rho \tag{29}$$

Using the elastic film shape in equation (4), the squeeze film term becomes:

$$\frac{\partial h}{\partial t} = \frac{\partial h_0}{\partial t} + \frac{\partial s}{\partial t} + \frac{\partial \delta}{\partial t} \tag{30}$$

where unlike most studied transient cases for bearings in normal approach or in reciprocating motions [20, 29, 51, 52], the contacting geometrical profile, s also alters in the case of meshing gear teeth, thus the instantaneous equivalent ellipsoidal solid of revolution in equations (5) and (6) is transitory. For small intervals of analysis, Δt:

$$\frac{\partial s}{\partial t} \cong \frac{s^n - s^{n-1}}{\Delta t} \tag{31}$$

Therefore, this term is also considered in the squeeze film motion in the current analysis, unlike in other reported analyses thus far.

Figure 2 shows the computational domain used in the current analysis where, f_i and f_o are the inlet and exit computational boundaries, whilst f_{s1} and f_{s2} are the set computational lateral boundaries.

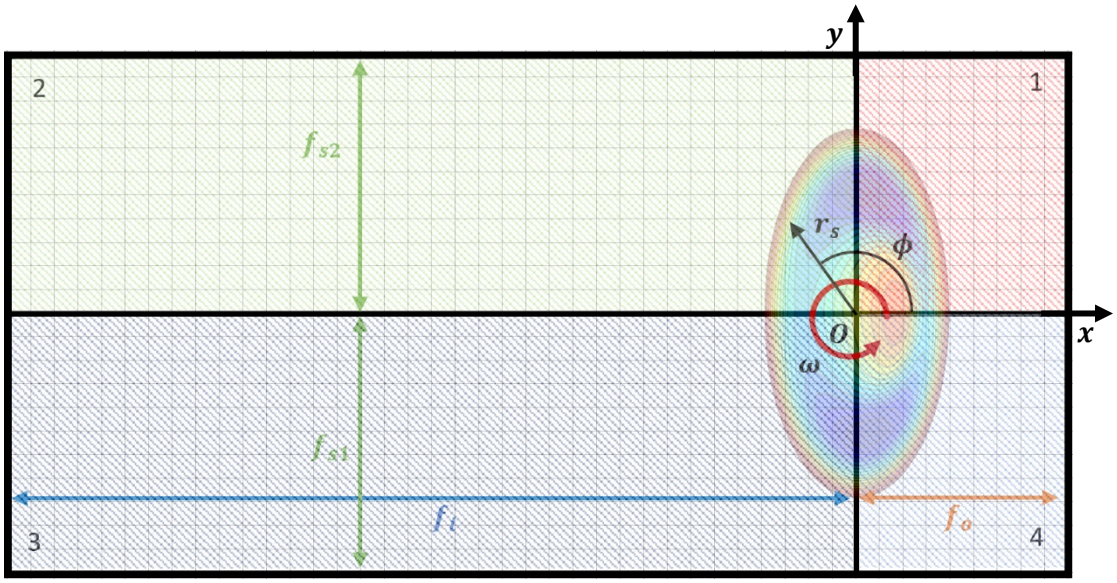

Figure 2: Computational boundaries and spin coordinates

Table 3 lists the inlet, exit and side leakage length parameters for the computational domain in Figure 2.

Table 3: Computational Domain

Parameter	Description	Value

f_i	Inlet distance	$6.5a$
f_o	Exit boundary	$1.5a$
f_{s1}, f_{s2}	Side Length	$1.5b$

In Figure 2 ω is the average angular spin of contact footprint in precession and r_s is the radial distance from the centre of the contact. Angle ϕ is the angle measured from the instantaneous minor axis of the elliptical point contact footprint. Thus, the additional flow velocities (due to spin) to those in equations (17) and (18) are [29]:

$$u_s = \omega r_s \sin\phi \tag{32}$$

$$v_s = \omega r_s \cos\phi \tag{33}$$

However, unlike in ref [29], where ω is given, at any time step n, here ω is found using:

$$\omega^n = \frac{{\Delta\theta_e}^n}{\Delta t} \tag{34}$$

where, Δt is the time step between successive mesh points and $\Delta\theta_e$ is the corresponding change in the angle of inlet flow entrainment at any step n, determined as:

$${\Delta\theta_e}^n = \tan^{-1}\left|\frac{V^n}{U^n}\right| - \tan^{-1}\left|\frac{V^{n-1}}{U^{n-1}}\right| \tag{35}$$

Thus, the overall surface velocities, depending on the computational quadrant in Figure 2 are evaluated. For example, for quadrant 1:

$$U_s = U - 2u_s \tag{36}$$

$$V_s = V + 2v_s \tag{37}$$

2.5- Friction: viscous and boundary contributions

Depending on the state of gears; new or extensively used, the composite root mean square (RMS) surface roughness of flank surfaces, σ_c resides between 0.1 µm and 0.45 µm [53]. In the current analysis, the RMS surface roughness of 0.2 µm used.

Total generated friction per meshing gear teeth pair comprises contributions due to shear of the lubricant film, as well as boundary friction because of the interacting counter face asperities, thus:

$$F_t = F_v + F_b \tag{38}$$

where, F_v and F_b are viscous and boundary friction contributions, respectively.

Viscous friction is obtained as:

$$F_v = \tau A_t \tag{39}$$

where, the shear stress, τ, under non-Newtonian behaviour is given as [41, 54]:

$$\tau = \frac{\eta}{F(\lambda)}\dot{\gamma} \tag{40}$$

Equation (39) is only valid when the calculated shear does not exceed the characteristic limiting shear stress of the lubricant, τ_0 (i.e., $\tau < \tau_0$) [54]. Otherwise, shear stress is dependent on the generated mean contact pressure [55, 56]:

$$\tau_l = \tau_0 + \vartheta \bar{p} \quad (41)$$

where, $\bar{p}$, is the average contact pressure and γ is the limiting shear strength proportionality constant.

The constant ϑ is found experimentally [56] and for synthetic oils is usually in the range: 0.026-0.04. To be consistent with the lubricant data used from Paouris et al [41]: $\vartheta = 0.029$.

Boundary friction is obtained as [55,57]:

$$F_b = \tau_0 A_{asp} + \varsigma W_{asp} \quad (42)$$

where, τ_0 is the Eyring shear stress and ς is the pressure coefficient of boundary shear strength of asperities on the softer of the counter faces (in this case both gears are made of steel). For high alloy steel of gearing: ς=0.17 [10, 52]. The total asperity contact area A_{asp} is [48]:

$$A_{asp} = \pi^2 (\xi_c \beta_c \sigma_c)^2 A_t F_2(\lambda_s) \quad (43)$$

where, the statistical function F_2 is found using a polynomial fit [57]:

$$F_2(\lambda_s) = -0.0018\lambda_s^5 + 0.0281\lambda_s^4 - 0.1728\lambda_s^3 + 0.5258\lambda_s^2 - 0.8043\lambda_s + 0.5003 \quad (44)$$

3- Simulated vehicular differential conditions

To investigate differential hypoid gear condition, a representative vehicular manoeuvre for a light duty commercial vehicle reported by Mohammadpour [10, 52] is used (Table 4). These correspond to vehicle speeds of 70 mph (for cruising on a highway) and 20 mph (for urban driving in congested traffic) respectively.

Table 4: Gear ratios with resulting RPM and torque [10, 52]

Gear No.	Ratio	Pinion RPM	Pinion Torque	Vehicle speed (mph)
2	2.038	324	732	20
5	0.702	118	2555	70

Xu et al [58] simulated a range of different engine torque-speed conditions to establish a range of differential gearing operating temperatures. The conditions chosen for the current analysis also fall within the range of conditions specified by Xu et al [58]. Therefore, an interpolated surface map is created as shown in Figure 3.

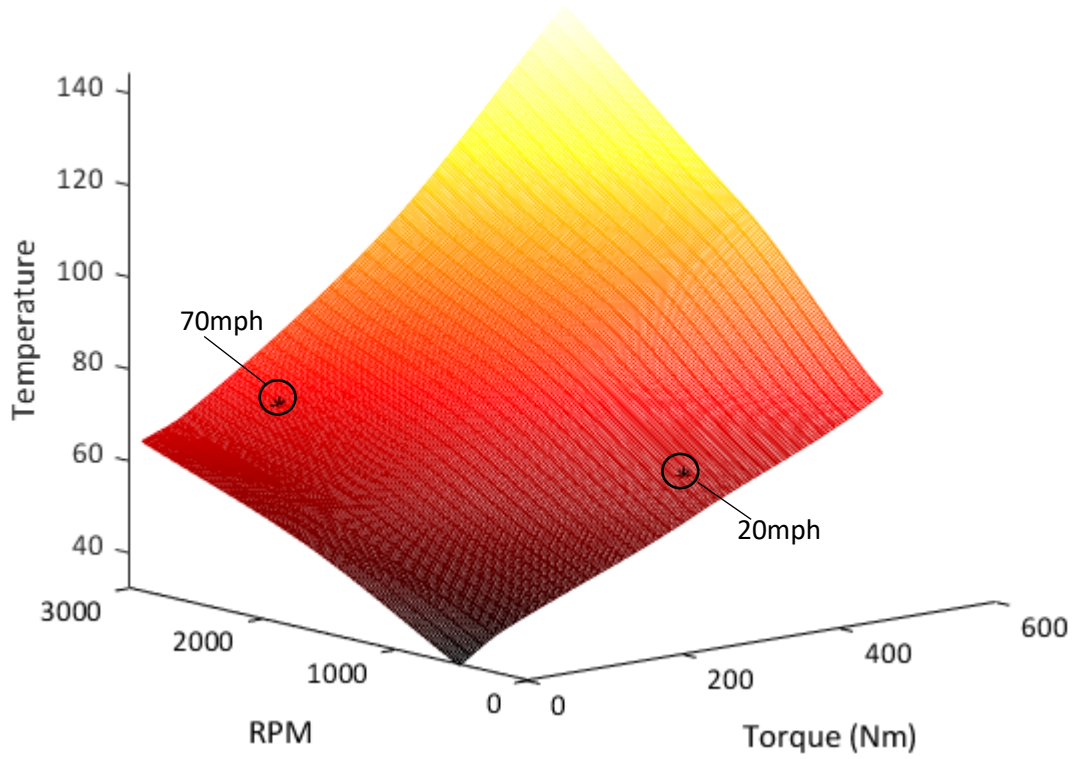

Figure 3: Interpolated surface map of temperature constructed from data of Xu et al [58]

It is expected that at 20 mph the lubricant's temperature reside between 40 °C and 60 °C, depending on the duration of vehicle motion [2]. Using Figure 3, the average temperature of approximately 63 °C is considered for vehicle speed of 20 mph. For the purpose of simulating cold start, the lower band of 40 °C is adopted instead.

Rheological properties of the lubricant are obtained for the two simulated vehicle conditions at the stated temperatures. These are listed in Tables 5 and 6.

Table 5: Lubricant properties for base temperature of 72 °C [49]

Parameter	Symbol	Value	Units
Dynamic viscosity	η_0	0.0295	$\mathrm{Pa.s}$
Pressure-viscosity coefficient	α_0	1.38×10^{-8}	Pa^{-1}
Density	ρ_0	798	$\mathrm{kg/m}^3$

Table 6: Lubricant properties for base temperature of 40 °C [49]

Parameter	Symbol	Value	Units

Dynamic viscosity	η_0	0.092	$\mathrm{Pa.\,s}$
Pressure-viscosity coefficient	α_0	1.60×10^{-8}	Pa^{-1}
Density	ρ_0	818	$\mathrm{kg/m}^3$

Using the approach highlighted above the non-Newtonian lubricant properties considered for the current analysis are listed in Table 7.

Table 7. Non-Newtonian lubricant properties [10]

Parameter	Value	Units
λ_f	7.9×10^{-8}	s
α_{HN}	0.7	-
β_{HN}	1.0	-

4. Results and Discussion

Figures 4(a) and 4(b) show the variations of predicted lubricant central contact and minimum exit film thickness for the vehicle speed of 70 mph (the speed limit on the UK motorway system). Both figures include the results from a quasi-static analysis which precludes the effect of squeeze film action. Squeeze film is present for the results under the more realistic transient contact conditions. It can be observed that the lubricant film thickness under all the differing analyses is quite thin, leading to mixed elastohydrodynamic regime of lubrication ($1 < \lambda_s < 3$). The lubricant film thickness is the least under the assumed quasi-static contact conditions owing to the omission of squeeze film effect, which enhances the load carrying capacity of the contact under transient conditions [28]. This is evident in the transient analysis with the inclusion of squeeze film velocity. When $\partial h/\partial t < 0$, mutual convergence of the surfaces (squeeze film action) occurs, resulting in an increase in both the central and minimum film thickness. In fact, a squeeze film cave (i.e., a dimple) is formed in the contact [51, 59]. This effect is shown in various parts of the meshing cycle in Figure 5. This is as the result of increased localised contact pressures at the same contact load relative to the case of quasi-static equilibrium. It should be noted that EHL films are to a large extent insensitive to load, but not to squeeze film action. When $\partial h/\partial t > 0$, contact separation occurs, which results in a drop in the lubricant film thickness with some delay due to the non-linear nature of EHL contacts. This is more noticeable in the variation of minimum film thickness in Figure 4(b), where the film thickness falls below the theoretical boundary lubrication demarcation line of $\lambda_s = 1$.

When spin is included in the analysis, both the lubricant central and minimum film thicknesses are reduced by an almost inappreciable amount because the proportion of lubricant entraining motion into the contact induced by spin is rather small (less than 20%) compared with that due to rolling-sliding motion of the meshing teeth (Figure 6). This is unlike the case reported by Mostofi and Gohar [11] under pure spin (i.e., accounting for 100% of the entraining motion).

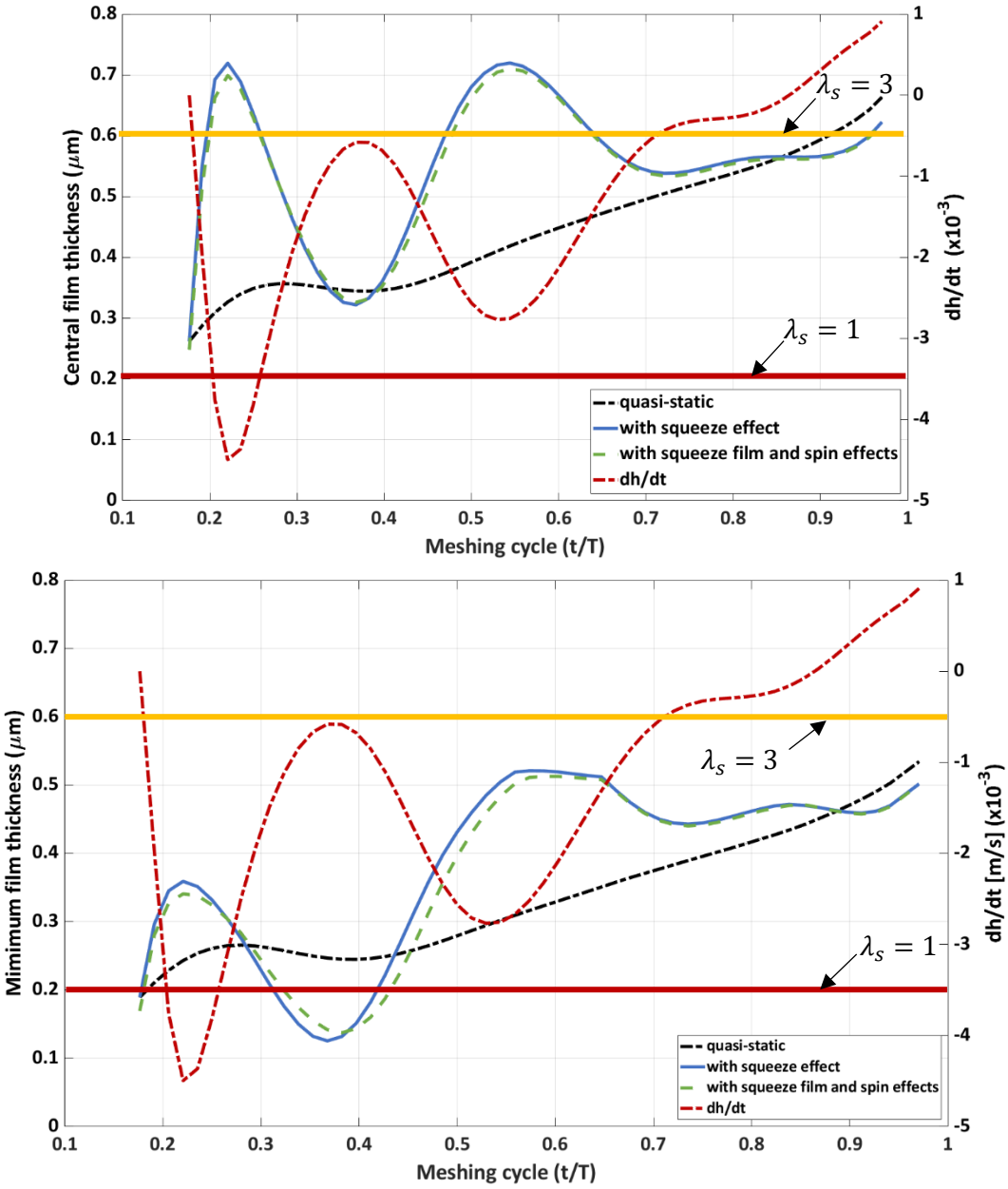

Figure 4: (a) Central and (b) minimum film thickness comparisons with squeeze film (transient) and also including contact footprint spin for vehicle speed of 70 mph

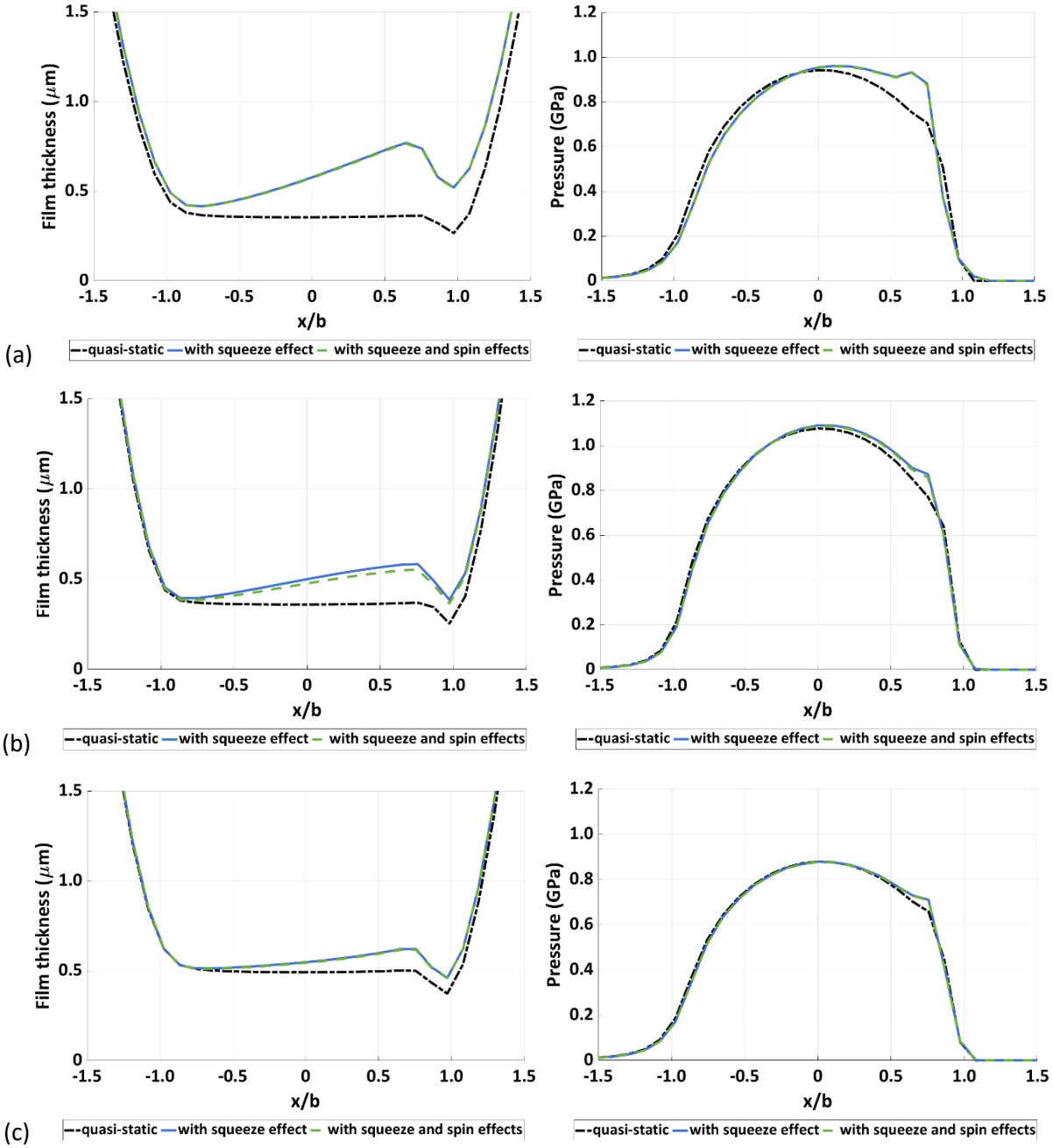

Figure 5: Centreline film shape (left) and corresponding pressure profile (right) for the vehicle speed of 70 mph at various instants of a meshing cycle, $\frac{t}{T}$: (a) 0.28, (b) 0.44, and (c) 0.70

Figure 6 shows that at the lower vehicle speed of 20 mph (with a lower rolling-sliding relative velocity of meshing teeth) the proportion of lubricant entraining motion due to any spinning motion increases, but only marginally.

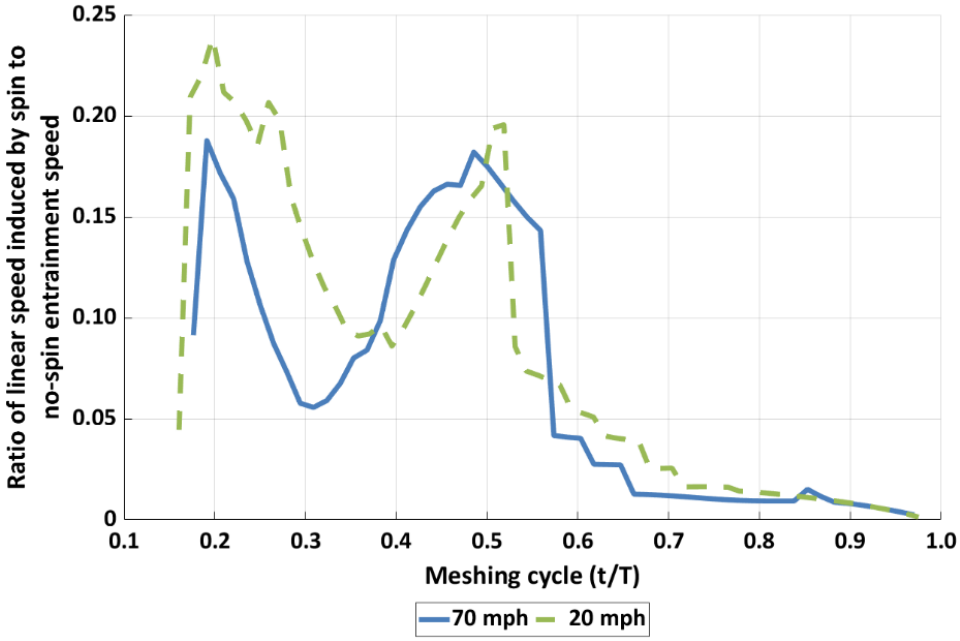

Figure 6: Ratio of linear speed induced by contact spin to the total lubricant entrainment velocity speed in a meshing cycle

The effect of spin is mostly on the oil film contour, resulting in asymmetrical film contours as shown in Figures 7-9 (corresponding to central film shapes in Figures 5 (a), (b) and (c)). The film thickness is generally enhanced under transient conditions, mainly due to the squeeze effect.

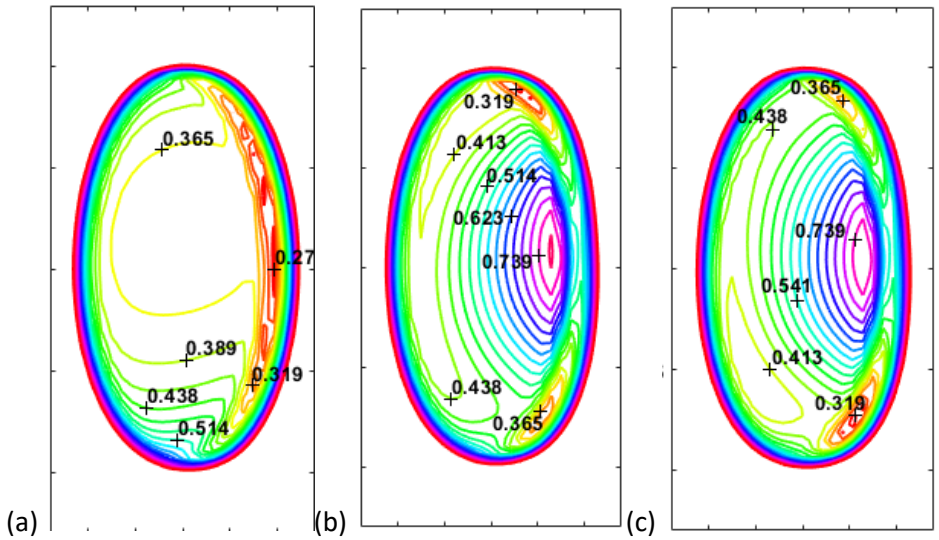

Figure 7: Film thickness contours (in μm) at $t/T = 0.28$ for 70 mph, (a) quasi-static, (b) transient with squeeze effect and (c) transient with squeeze effect and contact precession (spin)

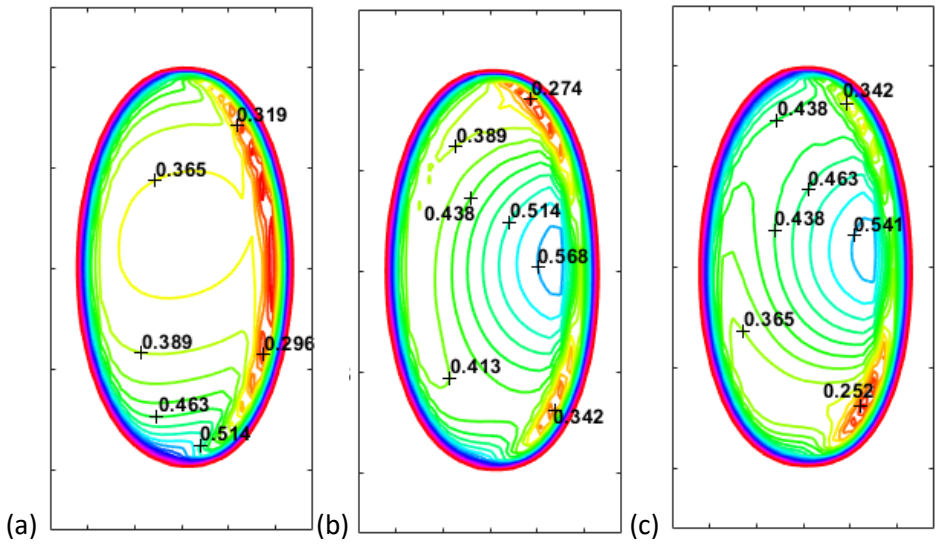

Figure 8: Film thickness contour (in µm) at $t/T = 0.44$ for 70 mph, (a) quasi-static, (b) transient with squeeze effect and c) transient with squeeze effect and contact precession (spin)

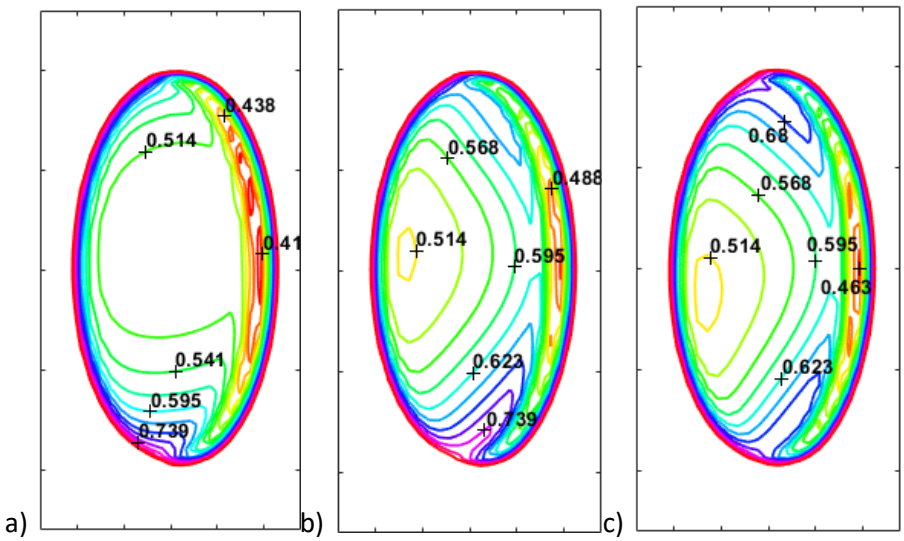

Figure 9: Film thickness contour (in µm) at $t/T = 0.70$ for 70 mph, (a) quasi-static, (b) transient with squeeze effect and (c) transient with squeeze effect and spin

At the vehicle cruising speed of 70 mph, the tribological contact conditions are more favourable than those prevailing at the vehicle speed of 20 mph corresponding to urban driving. The speed of entraining motion of the lubricant into the contact is higher at the cruising speed. Also, a lower contact load is carried by meshing teeth pairs at the higher cruising speed (Figures 10 and 11). Worse tribological conditions occur under mixed EHL regime of lubrication at high loads and lower speeds of entraining motion, therefore under urban driving conditions in this instance.

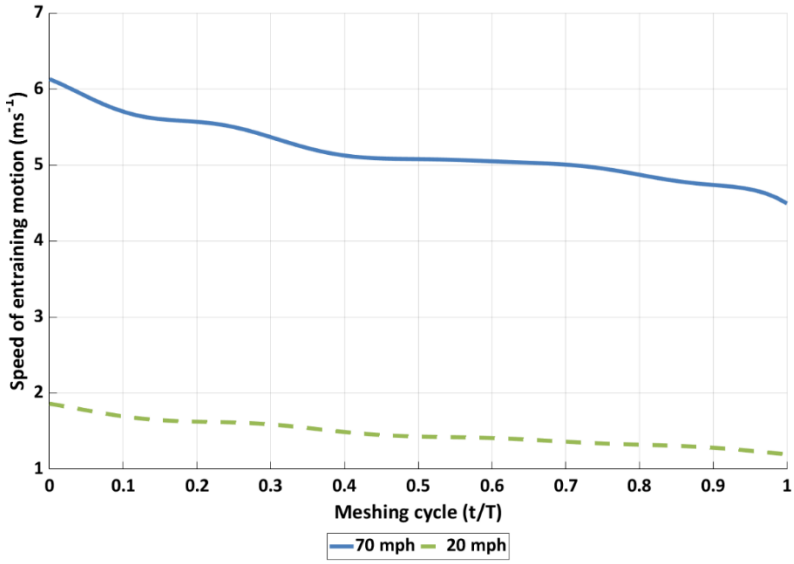

Figure 10: Speed of lubricant entraining motion in a meshing cycle in vehicle highway cruising and urban driving conditions

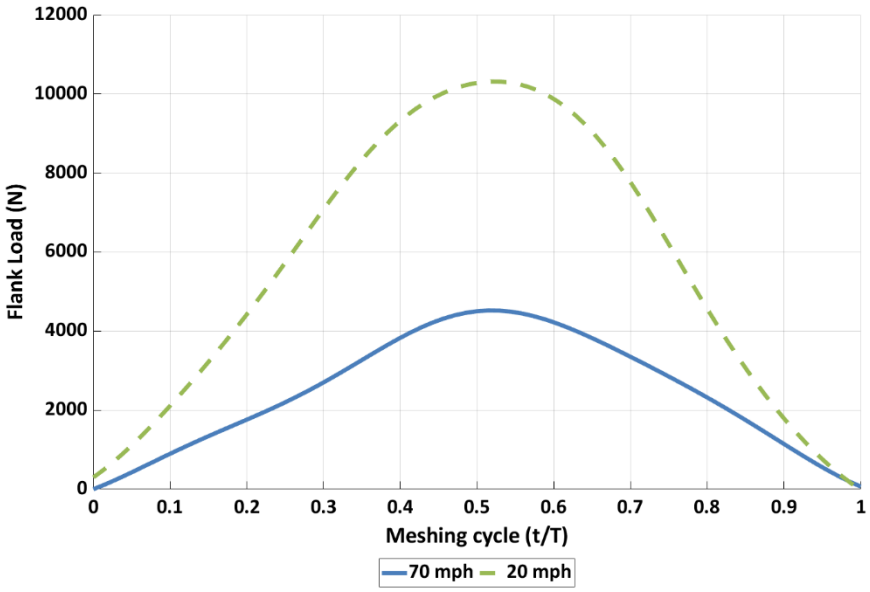

Figure 11: Contact load during a meshing cycle in vehicle highway cruising and urban driving conditions

Therefore, under urban driving one would expect harsher contact conditions and lower lubricant film thickness. The variation in the minimum oil film thickness is shown for a meshing cycle in Figure 12. The same overall observations can be made as in the case of the results for the vehicle cruising speed of 70 mph. The lubricant film thickness is reduced compared with that under the cruising speed of 70 mph

(Figure 4(b)) by approximately 15-20%. This is clearly due to the decreased speed of entraining motion of the lubricant into the contact. As a consequence, a longer period of boundary regime of lubrication occurs during the meshing cycle.

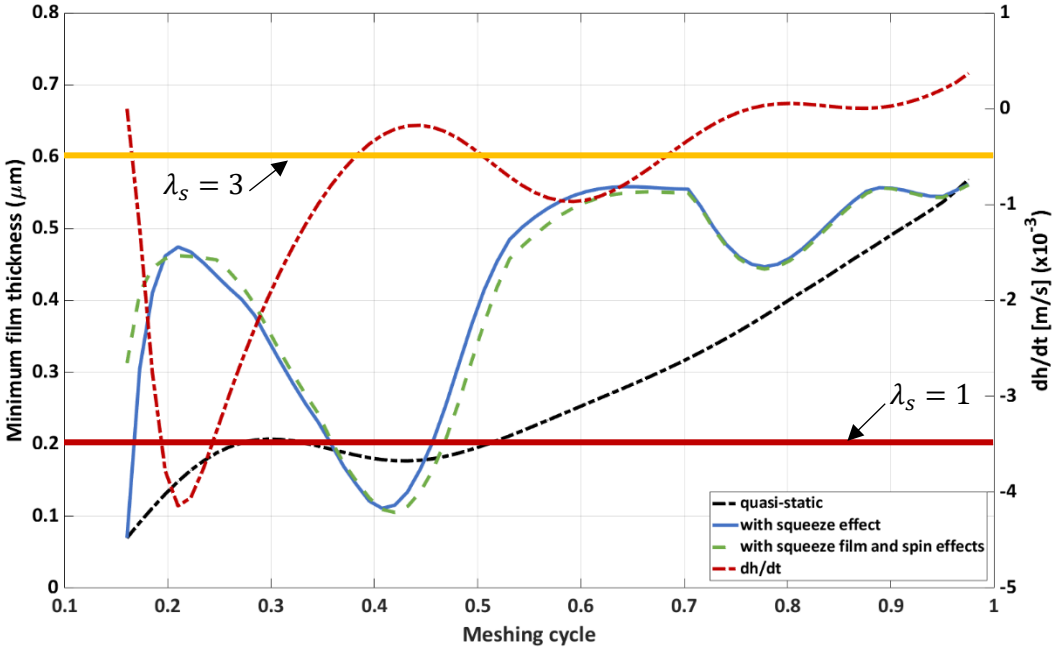

Figure 12: Minimum film thickness under various analysis methods for the vehicle speed of 20 mph

Figure 13 shows the corresponding film shape during parts of the meshing cycle. As in the previous case the squeeze film action can result in a cave or dimple which is quite dramatic at some instances as shown in Figure 13(a). The results also show the absence of any squeeze cave under quasi-static analysis as well as the diminution of the pressure spike at the contact exit.

Although the minimum film thickness falls below the surface roughness RMS of the contiguous meshing teeth pair surfaces (i.e., demarcation line; $\lambda_s = 1$ in Figures 4(b) and (12)) for both vehicle speeds of 20 and 70 mph, the proportion of contact in direct boundary interactions is actually minute, with boundary friction contribution being less than 0.5% of the overall contact friction. Figure 14 shows the overall friction variation in a meshing cycle for both the vehicle speeds considered in this study. As expected, friction is higher under urban driving condition at vehicle speed of 20 mph than at the cruising speed of 70 mph because of lower speed of lubricant entraining motion in the contact whilst carrying a larger generated torque.

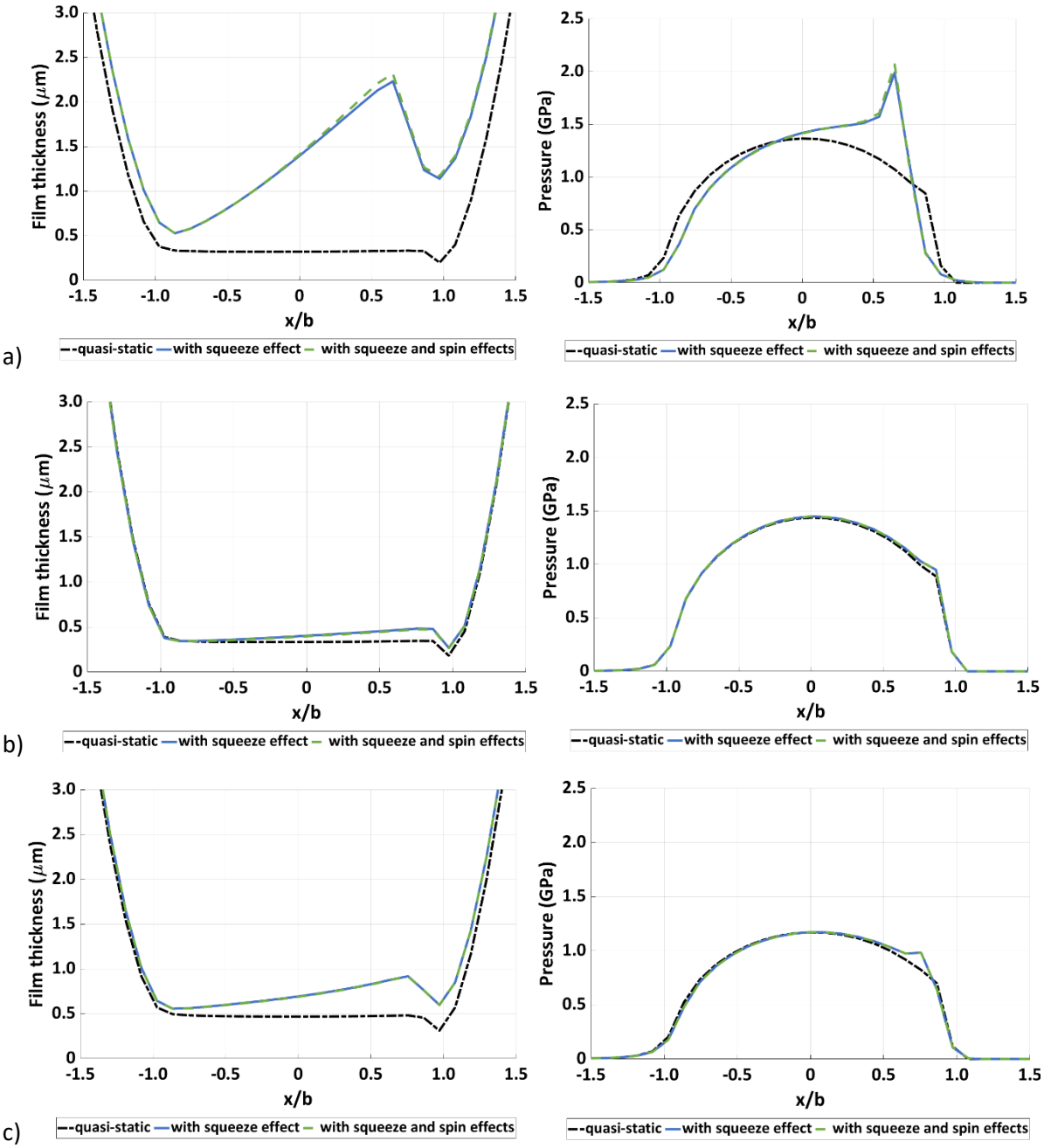

Figure 13: Centreline film thickness (left) and the corresponding pressure profile (right) for the vehicle speed of 20 mph at different instances of meshing cycle: t/T = a) 0.28, b) 0.44, and c) 0.70

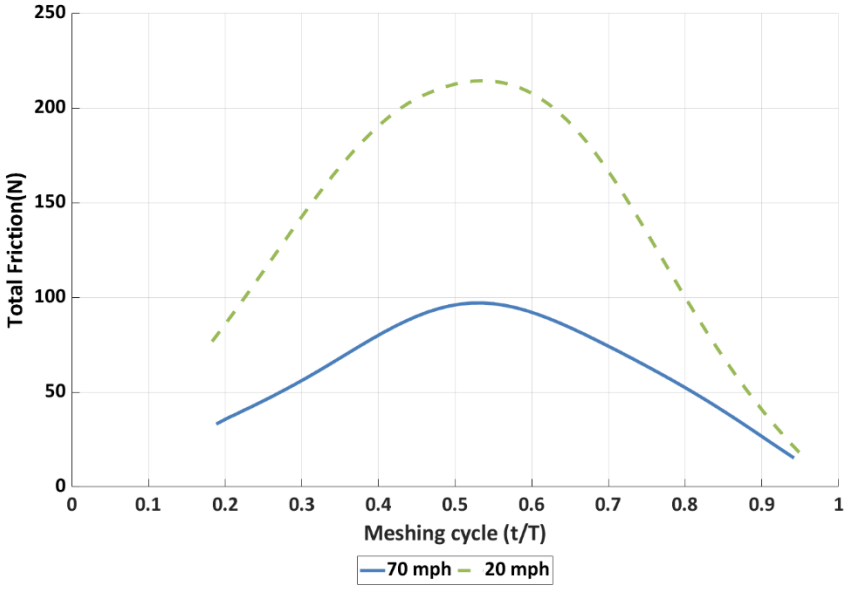

Figure 14: Generated total friction in a teeth pair contact during a meshing cycle

Referring to Figures 11 and 14 one can observe that the coefficient of friction varies between 0.02 and 0.025, indicating the predominance of viscous friction under the prevailing elastohydrodynamic regime of lubrication. Figure 15 shows that the lubricant is subjected to non-Newtonian traction throughout the meshing cycle, both in urban driving and under motorway cruising conditions as the shear stress remains in excess of the characteristic limiting shear stress of 4 MPa for the transmission fluid used in the current study.

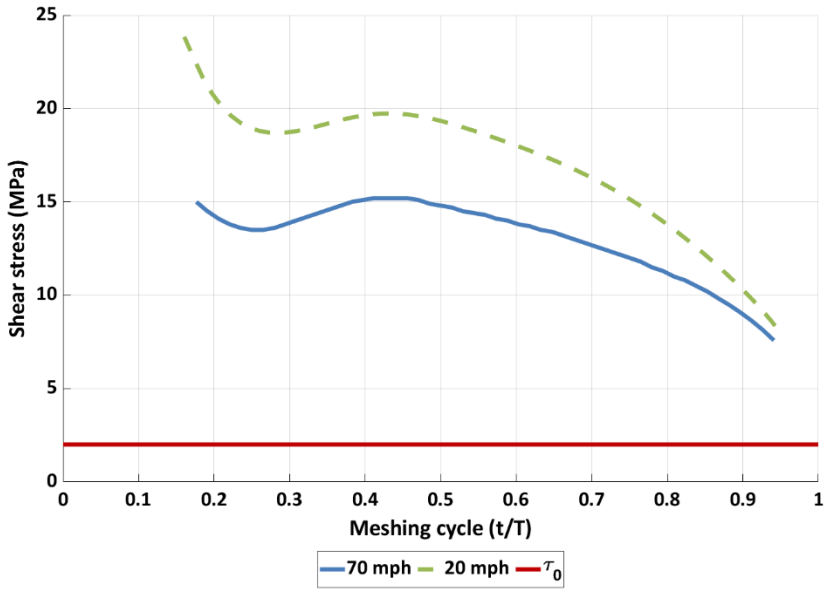

Figure 15: Non-Newtonian lubricant shear stress variation in a meshing cycle

Although the generated contact friction is higher under urban driving condition, the frictional power loss is larger under the higher speed cruising because the power loss is a function of both friction and the sliding speed of meshing teeth flanks as:

$$P_l = F_t \Delta U \tag{45}$$

where:

$$\Delta U = \sqrt{\left(u_p - u_g\right)^2 + \left(v_p - v_g\right)^2} \tag{46}$$

Figure 16 shows the power loss during a meshing cycle under both urban driving and high-speed cruising conditions.

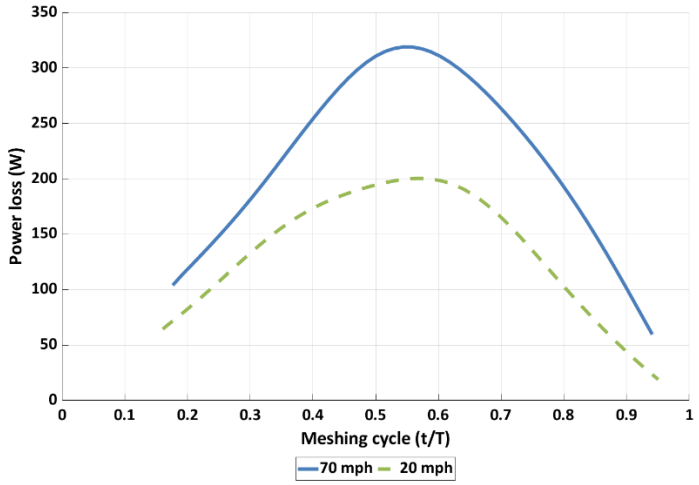

Figure 16: Power loss variation for a teeth pair contact during a meshing cycle

5. Conclusions

The findings of the current study demonstrate that any realistic analysis should include appropriate contact kinematics under transient conditions. In particular, the inclusion of squeeze film motion in the mutual convergence and separation of the meshing teeth pairs retains the history of the analysis, as well as taking into account its significant effect upon the transient load carrying capacity of the contact. Enhanced lubricant film thickness is noted due to the presence of a squeeze cave under realistic transient conditions which is absent in the case of predictions made using steady state or quasi-static analyses. It is also important to note the angled flow entrainment into the elliptical point contact footprint, affecting the side leakage from the contact and can result in a spin effect. This may be viewed as a contact footprint precession with the effect of an asymmetrical lubricant film distribution in the contact, affecting the position of the minimum film thickness. However, the effect of spin upon magnitude of film thickness is only marginal as it contributes less than 15-20% to the inflow in the direction of entraining motion.

Another important finding is that for a variety of vehicle operating conditions, from low-speed urban driving to highway cruising, the lubricant remains in non-Newtonian traction. It is also clear that including realistic run-in surface topography shows a very marginal effect upon boundary friction. Although in some other studies boundary regime of lubrication has been found to play a more significant role for some gearing systems, including for hypoid gears with different roughness patterns [60, 61]. The boundary friction model used in the current study is based on the work of Greenwood and Tripp [48] with reported measurements by Paouris et al [35,49]. Greenwood and Tripp [48] assumed a Gaussian distribution of asperity peaks. This is not usually the case for gear teeth surfaces unless for fairly smooth run-in cases as in the current analysis. For non-Gaussian distribution of asperity peaks Leighton et al [62] describe a surface-specific model, which can be adopted for future expansion of the current model, also taking into account the evolution of the surface topography through wear. The current study shows that for realistic vehicle conditions the regime of lubrication is non-Newtonian transient thermo-elastohydrodynamics with complex contact kinematics, comprising rolling, sliding, squeeze and spin actions. The inclusion of these complex kinematics, non-Newtonian rheological model, and realistic vehicle conditions account for the original contributions of this study. Clearly, more detailed thermal analysis, including the solution of energy equation would enhance the in-depth analysis as already shown in [8, 63, 64] including the nonlinearities that may arise in the dynamic response of the gear pair due to the transient effects [65].

Acknowledgments

The authors would like to express their gratitude to the Engineering and Physical Sciences Research Council (EPSRC) for the financial support of this research under the Centre for Doctoral Training for Embedded Intelligence (CDT-EI); grant reference: EP/L014998/1.

References:

[1]- Mohammadpour, M., Theodossiades, S., Rahnejat, H. and Kelly, P., “Transmission efficiency and noise, vibration and harshness refinement of differential hypoid gear pairs”, Proc. IMechE, Part K: J. Multi-body Dynamics, 2014, 228(1), pp. 19-33.

[2]- Koronias, G., Theodossiades, S., Rahnejat, H. and Saunders, T., “Axle whine phenomenon in light trucks: a combined numerical and experimental investigation”, Proc. IMechE, Part D: J. Automobile Engineering, 2011, 225(7), pp. 885-894.

[3]- Rahnejat, H., Rahmani, R., Mohammadpour, M. and Johns-Rahnejat, P.M., “Tribology of power train systems”, In ASM Handbook: Friction, Lubrication, and Wear Technology, ASM Int., 2017, 18, pp. 916–934.

[4]- Xu, H. and Kahraman, A., “Prediction of friction-related power losses of hypoid gear pairs”, Proc. IMechE, Part K: J. Multi-body Dynamics, 2007, 221(3), pp.387–400.

[5]- Simon, V. V., “Optimal Tooth Modifications in Face-Hobbed Spiral Bevel Gears to Reduce the Influence of Misalignments on Elastohydrodynamic Lubrication”, J. Mech. Des., 2014, 136(7): 071007.

[6]- Simon, V. V., “Improvements in the mixed elastohydrodynamic lubrication and in the efficiency of hypoid gears”, Proc. IMechE, Part J: J. Engineering Tribology, 2020, 234(6), pp.795–810.

[7]- Mohammadpour, M., Theodossiades, S. and Rahnejat, H., “Elastohydrodynamic lubrication of hypoid gear pairs at high loads”, Proc. IMechE, Part J: J. Engineering Tribology, 2012, 226(3), pp.183–198.

[8]- Mohammadpour, M., Theodossiades, S., Rahnejat, H. and Dowson, D., “Non-Newtonian mixed thermo-elastohydrodynamics of hypoid gear pairs”, Proc IMechE, Part J: J. Engineering Tribology, 2018, 232(9), pp.1105–1125.

[9]- Chittenden, R.J., Dowson, D., Dunn, J.F. and Taylor, C.M., “A Theoretical Analysis of the Isothermal EHD Lubrication of Concentrated Contact. II: General Case with Lubricant Entrainment along Either Principal Axis of the Hertzien Contact Ellipse or at Some Intermediate Angle”, Proc. Roy. Soc. London, 1985, 397, pp.271-294.

[10]- Mohammadpour, M., Theodossiades, S. and Rahnejat, H., “Transient mixed non-Newtonian thermo-elastohydrodynamics of vehicle differential hypoid gears with starved partial counter-flow inlet boundary”, Proc. IMechE, Part J: J. Engineering Tribology, 2014, 228(10), pp.1159-1173.

[11]- Mostofi, A. and Gohar, R., “Oil Film Thickness and Pressure Distribution in Elastohydrodynamic Point Contacts”, Proc. IMechE, Part C; J. Mechanical Engineering Science, 1982, 24(4), pp.173–182.

[12]- Ehret, P., Chevalier, F., Dowson, D., Taylor, C.M., Okamura, H. and Sano, T., “Traction in EHL elliptical contacts with spin conditions”, Tribology Series, 2000, 38, pp.71-83.

[13]- Li, X.M., Guo, F., Fan, B. and Yang, P., “Influence of spinning on the rolling EHL films” Tribology Int., 2010, 43(11), pp.2020–2028.

[14]- Dormois, H., Fillot, N., Habchi, W., Dalmaz, G., Vergne, P., Morales-Espejel, G.E. and Ioannides, E., “A Numerical Study of Friction in Isothermal EHD Rolling-Sliding Sphere-Plane Contacts with Spinning”, J. Tribology, 2010, 132(2): 021501.

[15]- Doki-Thonon, T., Fillot, N., Morales-Espejel, G.E., Querry, M., Philippon, D., Devaux, N. and Vergne, P.A., “Dual Experimental/Numerical Approach for Film Thickness Analysis in TEHL Spinning Skewing Circular Contacts”, Tribology Letters, 2013,50(1), pp.115–126.

[16]- Yan, X., Zhang, Y., Xie, G., Qin, F. and Zhang, X., “Effects of spinning on the mixed thermal elastohydrodynamic lubrication and fatigue life in point contacts”, Proc. IMechE, Part J: J. Engineering Tribology, 2019, 233(12), pp.1820-1832.

[17]- Christensen, H., “Elastohydrodynamic Theory of Spherical Bodies in Normal Approach”, J. Lubrication Technology, 1970, 92(1), pp.145–153.

[18]- Herrebrugh, K., “Elastohydrodynamic Squeeze Films Between Two Cylinders in Normal Approach”, J. Lubrication Technology, 1970, 92(2), pp.292–301.

[19]- Ren, N., Zhu, D. and Wen, S.Z., “Experimental method for quantitative analysis of transient EHL”, Tribology International, 1991, 24(4), pp. 225-230.

[20]- Jalali-Vahid, D., Rahnejat, H. and Jin, Z.M., “Elastohydrodynamic solution for concentrated elliptical point contact of machine elements under combined entraining and squeeze-film motion”, Proc. IMechE, Part J: J. Engineering Tribology, 1998, 212(6), pp.401-411.

[21]- Dowson, D. and Jones, D.A., “Lubricant entrapment between approaching elastic solids”, Nature, 1967, 214(5091), pp. 947-948.

[22]- Safa, M. M. A. and Gohar, R., "Pressure distribution under a ball impacting a thin lubricant layer", J. Tribology, 1986, 108(3), pp. 372-376.

[23]- Gohar, R. and Safa M.M.A., “Measurement of contact pressure under elastohydrodynamic lubrication conditions”, In Tribology and Dynamics of Engine and Powertrain, 2010, pp. 222-245

[24]- Al-Samieh, M.F. and Rahnejat, H., “Physics of lubricated impact of a sphere on a plate in a narrow continuum to gaps of molecular dimensions”, J. Physics, D: Applied Physics, 2002, 35(18):2311.

[25]- Venner, C.H., Wang, J. and Lubrecht, A.A., „Central film thickness in EHL point contacts under pure impact revisited”, Tribology international, 2016, 100, pp. 1-6.

[26]- Larsson, R., “Transient non-Newtonian elastohydrodynamic lubrication analysis of an involute spur gear”, Wear, 1997, 207(1–2), pp.67–73.

[27]- Wang, J., Hashimoto, T., Nishikawa, H. and Kaneta M., “Pure rolling elastohydrodynamic lubrication of short stroke reciprocating motion”, Tribology International, 2005, 38(11-12), pp. 1013-1021.

[28]- Gohar, R. and Rahnejat, H., “Fundamentals of Tribology”, Imperial College Press, London, 2008.

[29]- Sivayogan, G., Rahmani, R. and Rahnejat, H., “Transient Analysis of Isothermal Elastohydrodynamic Point Contacts under Complex Kinematics of Combined Rolling, Spinning and Normal Approach”, Lubricants, 2020, 8(8):81.

[30]- Sivayogan, G., Rahmani, R. and Rahnejat, H., “Lubricated loaded tooth contact analysis and non-Newtonian thermoelastohydrodynamics of high-performance spur gear transmission systems”, Lubricants, 2020, 8(2):20.

[31]- Li, S. and Kahraman, A., “Prediction of spur gear mechanical power losses using a transient elastohydrodynamic lubrication model”, Tribology Transactions, 2010, 53(4), pp.554–563.

[32]- Li, S. and Kahraman, A., “A Transient Mixed Elastohydrodynamic Lubrication Model for Spur Gear Pairs”, J. Tribology, 2010, 132(1): 011501.

[33]- Li, S. and Kahraman, A., “Influence of dynamic behaviour on elastohydrodynamic lubrication of spur gears”, Proc. IMechE, Part J: J. Engineering Tribology, 2011, 225(8), pp.740–753.

[34]- Mohammadpour, M., Theodossiades, S. and Rahnejat, H., "Multiphysics Investigations on the Dynamics of Differential Hypoid Gears", J. Vibration and Acoustics, 2014, 136(4): 041007.

[35]- Paouris, L., Rahmani, R., Theodossiades, S., Rahnejat, H., Hunt, G. and Barton, W., "Inefficiency predictions in a hypoid gear pair through tribodynamics analysis", Tribology International, 2018, 119, pp.631–644.

[36]- Bobach, L., Beilicke, R. and Bartel, D., "Transient thermal elastohydrodynamic simulation of a spiral bevel gear pair with an octoidal tooth profile under mixed friction conditions", Tribology International, 2020, 143: 106020.

[37]- Merritt, H.E., "Gears", Pitman, London, 1954.

[38]- Rahnejat, H. and Johns-Rahnejat, P.M., "Mechanics of contacting surfaces", Encyclopedia of Automotive Engineering, 2014, 17:1-9.

[39]- Habchi, W., Eyheramendy, D., Bair, S., Vergne, P. and Morales-Espejel, G., "Thermal elastohydrodynamic lubrication of point contacts using a Newtonian/generalized Newtonian lubricant", Tribology letters, 2008, 30(1):41.

[40]- Havriliak, S. and Negami, S., "A complex plane representation of dielectric and mechanical relaxation processes in some polymers", Polymer, 1967, 8, pp.161–210.

[41]- Paouris, L., Rahmani, R., Theodossiades, S., Rahnejat, H., Hunt, G. and Barton, W., "An analytical approach for prediction of elastohydrodynamic friction with inlet shear heating and starvation", Tribology Letters, 2016, 64(1), pp. 1-8.

[42]- Roelands, C.J.A., "Correlational aspects of the viscosity-temperature-pressure relationship of lubricating oils", PhD Thesis, Delt University of Technology, 1966.

[43]- Vogel, H., "The law of the relation between the viscosity of liquids and the temperature", Phys. Z., 1921, 22, pp. 645-646.

[44]- Yang, P., Cui, J., Jin, Z.M. and Dowson, D., "Transient elastohydrodynamic analysis of elliptical contacts; Part 2: thermal and Newtonian lubricant solution", Proc. IMechE, Part J: J. Engineering Tribology, 2005, 219(3), pp. 187-200.

[45]- Litvin, F.L. and Fuentes, A., "Gear geometry and applied theory", Cambridge University Press, 2004, Cambridge, UK.

[46]- Vijayakar, S., "Tooth contact analysis software: calyx", Advanced Numerical Solutions, Hilliard, 1998, OH, USA.

[47]- Karagiannis, I., Theodossiades, S. and Rahnejat, H., "On the dynamics of lubricated hypoid gears", Mechanism and Machine theory, 2012, 48, pp. 94-120.

[48]- Greenwood, J.A. and Tripp, J.H., "The Contact of Two Nominally Flat Rough Surfaces", Proc. IMechE, 1970, 185(1), pp.625–633.

[49] Paouris. L., “Thermo-elastohydrodynamics of hypoid gears with formulated lubricants”, PhD Thesis, Loughborough University, 2016, UK.

[50]- Teodorescu, M., Balakrishnan, S. and Rahnejat, H., “Integrated tribological analysis within a multi-physics approach to system dynamics”, In Tribology and Interface Engineering Series, 2005, 48, pp. 725-737.

[51]- Dowson, D. and Wang, D., “An analysis of the normal bouncing of a solid elastic ball on an oily plate”, Wear, 1994, 179(1-2), pp. 29-37.

[52]- Mohammadpour, M., Theodossiades, S., Rahnejat, H. and Saunders, T., “Non-Newtonian mixed elastohydrodynamics of differential hypoid gears at high loads”, Meccanica, 2014, 49(5), pp.1115–1138.

[53]- Kolivand, M., Li, S. and Kahraman, A., “Prediction of mechanical gear mesh efficiency of hypoid gear pairs”, Mech Mach Theory, 2010, 45(11), pp.1568–1582.

[54]- Evans, C.R. and Johnson, K.L., “Regimes of traction in elastohydrodynamic lubrication”, Proc. IMechE, Part C: J. Mech. Eng. Sci., 1986, 200(5), pp.313-324.

[55]- Briscoe, B.J. and Evans, D.C., “The shear properties of Langmuir—Blodgett layers”, Proc. Roy. Soc., Ser. A., 1982, 380(1779), pp. 389-407.

[56]- Höglund, E. and Jacobson, B., “Experimental Investigation of the Shear Strength of Lubricants Subjected to High Pressure and Temperature”, J Tribology, 1986,108(4), pp. 571–577.

[57]- De La Cruz, M., Chong, W.W.F., Teodorescu, M., Theodossiades, S. and Rahnejat, H., “Transient mixed thermo-elastohydrodynamic lubrication in multi-speed transmissions”, Tribology International, 2012, 49, pp.17–29

[58]- Xu, H., Singh, A., Maddock, D., Kahraman, A. and Hurley, J., “Thermal mapping of an automotive rear drive axle”, SAE Int., J. Engines, 2011, 4(1), pp. 888-901.

[59]- Kushwaha, M. and Rahnejat, H., “Transient concentrated finite line roller-to-race contact under combined entraining, tilting and squeeze film motions”, J. Physics, D: Applied Physics, 2004, 37(14), p. 2018.

[60]- Huang, D., Wang, Z., Li, G. and Zhu, W., “Conjugate approach for hypoid gears frictional loss comparison between different roughness patterns under mixed elastohydrodynamic lubrication regime”, Tribology International, 2019,140:105884.

[61]- Wang, C., and Mao K., "A calculation method of sliding friction coefficient on tooth surface for helical gear pair based on loaded tooth contact analysis and elastohydrodynamic lubrication theory." Proc. IMechE, Part J: J. Engineering Tribology, 2021, 235(8): 1551-1560.

[62]- Leighton, M., Morris, N., Gore, M., Rahmani, R., Rahnejat, H. and King, P.D., “Boundary interactions of rough non-Gaussian surfaces”, Proc. IMechE, Part J: J. Engineering Tribology, 2016, 230(11), pp. 1359-1370.

[63]- Simon, V. "Elastohydrodynamic lubrication of hypoid gears", J. Mech. Des., 1981, 103(1), pp. 195-203.

[64]- Peiran, Y. and Shizhu, W., “A generalized Reynolds equation for non-Newtonian thermal elastohydrodynamic lubrication”, J. Tribology, 1990, 112, pp. 631–636.

[65]- Wang, Z., Wei P., Xin P., and Wei C., "Nonlinear dynamical behaviors of spiral bevel gears in transient mixed lubrication.", Tribology International, 2021, 160:107022.

Nomenclature

$\hat{a}, \hat{b}$	Unit vectors along the major and minor axes of the contact footprint
A_{asp}	Total asperities’ contact area
A_t	Wetted contact area)
a_v, b_v, c_v	Vogel constants
$E_{1,2}$	Young’s moduli of elasticity of the contacting pairs
E'	Reduced Young’s modulus of elasticity: $(2/[(1-\nu_1^2)/E_1 + (1-\nu_2^2)/E_2)$
E_p, E_w	Convergence criteria for pressure and load
$F_2, F_{5/2}$	Statistical function
F_b	Boundary friction
F_t	Total friction
F_v	Viscous friction
f_i, f_o	Computational domain inlet and exit boundary lengths
f_{s1}, f_{s2}	Computational domain side lengths
h	Film thickness
h_0	Rigid minimum clearance
h_c	Central film thickness
h_m	Minimum film thickness
i, j	Node position
$\hat{k}_{s_i}$	Axis of rotation unit vectors with s_i denoting pinion p or gear g
M	Transformation matrix
n	Iteration step number

P_l	Power loss
p	Pressure
$\bar{p}$	Average contact pressure
R_{x1}, R_{x2}	Radii of curvature along the minor axis of the contacting teeth flanks
R_{y1}, R_{y2}	Radii of curvature along the major axis of the contacting teeth flanks
R_{zx}, R_{zy}	Principal radii of the equivalent ellipsoidal solid
$\overline{r_p}, \overline{r_g}$	Position vector of pinion and wheel respectively
r_s	Radial distance
s	Geometric profile
T	Time period for a meshing cycle
T_0	Atmospheric base reference temperature
t	Time
U	Surface speed along minor axis $(u_p + u_g)$
ΔU	Sliding speed of meshing teeth flanks
u_p, u_g	Surface speed along the minor axis of the pinion and the wheel respectively
u_s	Surface speed along the minor axis under pure spin
u_{s_i}	Generalised surface speed along major axis, with s_i denoting pinion p or gear g
V	Surface speed along major axis $(v_p + v_g)$
v	Entrainment speed along the major axis $((v_p + v_g)/2)$
v_p, v_g	Surface speed along the major axis of pinion and wheel respectively
v_s	Surface speed along major axis under pure spin
v_{s_i}	Generalised surface speed along major axis, with s_i denoting pinion p or gear g
W	Flank load
W_{asp}	Load carried by the asperities
W_l	Load carried by the lubricant
W_p	Load carried by the lubricant
W_t	Total computed load in the contact $(W_p + W_{asp})$
x, y	Cartesian coordinate set

x', y'	Coordinates of pressure application points
Z	Piezoviscosity index

Greek Symbols

α_0	Piezo-viscosity coefficient at ambient temperature
α_{HN}, β_{HN}	Havriliak and Negami parameters
β_c	Average radius of curvature of asperity tips
$\dot{\gamma}$	Lubricant shear rate
δ	Local elastic deflection
ζ	Load relaxation factor
η	Lubricant dynamic viscosity
η_e	Effective dynamic viscosity
η_0	Viscosity at ambient temperature and pressure
η_p	Modified viscosity
η_r, p_r	Roeland's viscosity constants
ϑ	Limiting shear-strength proportionality constant
θ	Lubricant entrainment angle into the contact with the minor axis
λ_f	Relaxation time
λ_s	Stribeck's Oil film parameter (h_c/σ_c)
$\upsilon_{1,2}$	Poisson's ratios of the contacting pairs
ξ_c	Asperity density per unit area
ρ	Lubricant density
ρ_0	Density at ambient temperature and pressure
σ_c	Combined RMS surface roughness
ς	Pressure coefficient of boundary shear strength
τ	Shear stress
τ_0	Eyring shear stress
τ_l	Limiting shear stress
ϕ	Angle between r_s and the minor axis
ω	Average angular spin velocity of contact footprint in precession

ω_p, ω_g	Angular velocity of pinion and wheel respectively
ω_{s_i}	Generalised angular velocity
Ω	Under-relaxation factor

Abbreviations

EHL	Elastohydrodynamic Lubrication
RMS	Root Mean Square
RPM	Revolutions per Minute
TCA	Tooth Contact Analysis